Laser Physics, Vol. 14, No. 5, 2004, pp. 1–8.

Enhanced Tunable Terahertz Generation in Photonic Band-Gap Structures

J. W. Haus[1], P. Powers[1], P. Bojja[1], M. Torres-Cisneros[1], M. Scalora[2], M. J. Bloemer2, N. Akozbek[3], and M. A. Meneses-Nava[4]

[1] *Electro-Optics Program, University of Dayton, Dayton, Ohio, 45469-0245 USA*
e-mail: Joseph.Haus@notes.udayton.edu
[2] *Weapons Sciences Directorate, AMSMI-RD-WS-ST, Research, Development and Engineering Center, U.S. Army Aviation and Missile Command, Huntsville, Alabama, 35898-5248 USA*
[3] *Time Domain Corp, Cummings Research Park, 7097 Old Madison Pike, Huntsville, Alabama, 35806 USA*
[4] *Optical Properties of Matter Group, Centro de Investigaciones en Optica, Loma del Pocito S/N, Leon GTO, Mexico*

Received October 17, 2003

Abstract—We analyze a novel coherent source of millimeter-wavelength waves based on parametric down conversion in a photonic crystal. Our design is based on the band-edge or defect-mode field enhancement phenomena near a photonic band gap. The numerical results show that a wide range of intensities and bandwidths of coherent radiation can be obtained as we vary either the number periods or the index contrast between layers of the crystal array. Calculations demonstrate narrow-band, continuous and tunable THz sources from sub-THz to more than 12 THz.

1. INTRODUCTION

At present, coherent source designs enable us to generate practically any frequency in microwave and in visible regions at different power levels. Nevertheless, between these wavelengths [from 10^{-6} to 10^{-3} meters], there has been considerable research activity and until recently only a few laser sources. At wavelengths corresponding to terahertz (THz) frequencies, there is clear evidence that such sources could be useful for an enormous number of imaging and sensing applications. Several techniques based on either novel schemes or exploiting well-known effects have been applied in order to develop THz sources. Each of these designs has different characteristics and works preferentially in a range of the wide THz region [0.1–10 THz]. The passive solid-state[1] source design is one of the best proposals for the low portion of the THz spectrum, although the most promising designs involve optical effects such as photoconductivity (PC)[2, 3], optical parametric oscillation (OPO) [4, 5], optical parametric generation (OPG) [6], optical rectification [7–10], photomixing [11, 12], and femtosecond pulse shaping [13]. Quantum cascade lasers [14] form another branch of active THz device development. These sources can generate THz frequencies with output powers ranging from milliwatts to nanowatts.

Some THz sources are currently being applied to specific technologies, such as coherent time-domain spectroscopy [15], T-wave imaging and ranging of objects [16, 17], dynamic analysis in semiconductors [18, 19], environment monitoring [20], and frequency standards [21]. Novel concepts have been proposed for potential applications to radar systems, optical communications, medical imaging, nonlinear spectroscopy, and so on. These applications would be enabled by the availability of THz sources. The sources must satisfy different criteria, depending on the specific application, such as being compact, tunable across a wide portion of the THz bands, having variable bandwidth or high power, or being inexpensive.

From all these proposals, perhaps the most widely applied is that based on optical rectification effects. The use of optical rectification or parametric down conversion is perhaps best illustrated by the use of periodic poled lithium niobate (PPLN) crystals. Some of the reasons for the popularity of PPLN are its simple experimental setup, its compact design, and its relatively narrow bandwidth, even though the quantum conversion efficiency is low, resulting in low output power [22]. Nevertheless, it is an appealing technique and the optical characteristics of the generated signal can be tailored crystals other than PPLN.

Structures where the interfering films are arranged with thicknesses that are comparable to the wavelength of the source are called photonic crystals or photonic band-gap (PBG) structures. They are designed to exploit the special properties that occur due to the interference among the layers. For instance, light transmission can be suppressed over a specific band of frequencies or the wave dispersion can be managed to reshape pulses or phase match multiple wavelength signals in a nonlinear material environment.

In a recent publication, Yan-qing Lu *et al.* [23] proposed the use of a nonlinear photonic crystal or PBG device to generate coherent microwave radiation through the optical rectification effect. They used the PBG dispersion characteristics in order to solve the

[1] On sabbatical leave from Electronics Dept, FIMEE, University of Guanajuato, Salamanca, Guanajuato. Mexico.

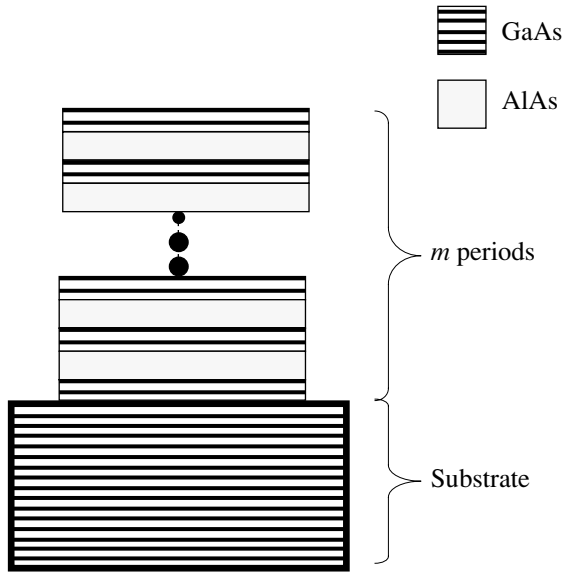

Fig. 1. Geometry array: m GaAs/AlAs periods deposited on a GaAs substrate. Each period consists of one GaAs layer followed by a second, lower index material; i.e., we consider a (AlAs, Al_2O_3, air) layer. The substrate thickness is assumed to be infinite.

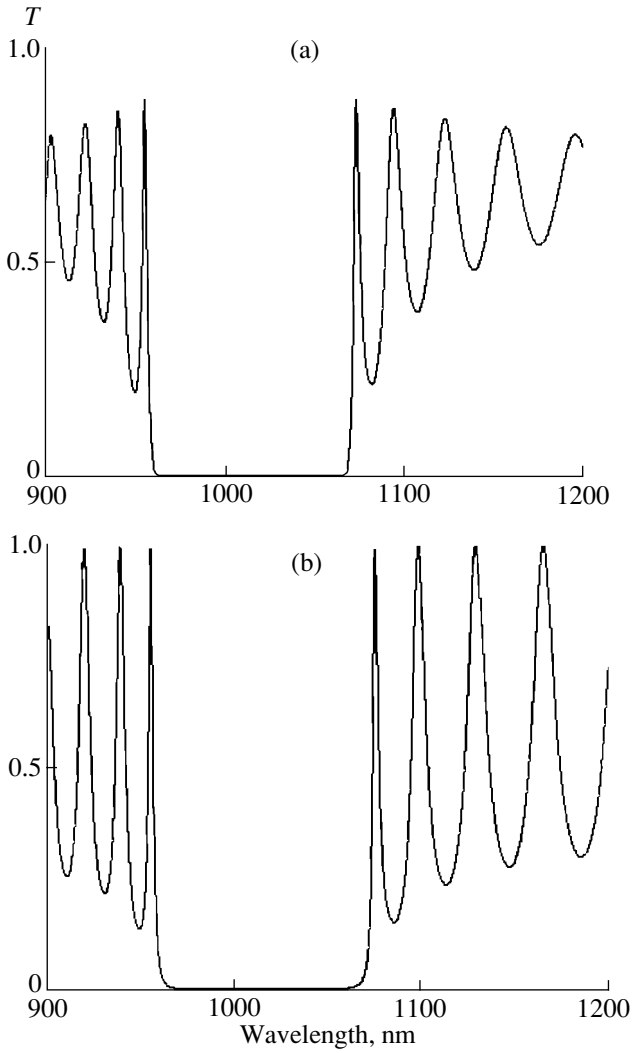

Fig. 2. Plots of the transmission spectra for 30 periods (60 layers) illustrating the effect of the substrate. Physical parameters are described in the text. The two materials are GaAs/AlAs on a. (a) GaAs substrate. (b) Air substrate.

phase-matching problem, but they did not consider the effects of band-edge enhancement nor did they discuss the effects of using sources at different incident angles to tune output THz radiation.

In this paper, we concentrate on the same problem of generating coherent THz radiation using a PGB structure, but we focus on the local-field enhancement mechanism that is available by tuning the driving fields either to the band edge or to a defect mode in the band gap. The local-field phenomenon involves resonant field enhancement and increased density of states or, equivalently, the slow group velocity of the optical waves [24]. The combination of these effects can provide great flexibility in the design of new devices for sub-THz or THz wave generation. We report an enhancement that is compared against the result expected for a homogeneous GaAs material of the same thickness. We also show that the enhancement is retained and the THz radiation is broadly tunable when the two laser sources are not colinear.

2. ANALYSIS

We looked at several geometries using GaAs as the first material and materials such as AlAs, Al_2O_3 (alumina), or air as the second material. Each pair provides a larger index contrast. The final optimized structure does not rely on GaAs for the nonlinear mixing to generate radiation.

Other materials, such as GaN or even poled electrooptic polymers, could be incorporated into final designs based on the availability of fabrication techniques.

The theoretical analysis involves the application of the transfer matrix method to compute the fields at two wavelengths inside the PBG structure that are detuned from one another to generate the desired difference frequency. Both driving fields are tuned near the same transmission resonance in the structure. The dispersive dielectric properties of the materials were incorporated into the program. We considered the possibility of air and GaAs substrates and comment on the effect of different substrates.

2.1. Band-Edge Enhancement

The simple one-dimensional PGB sample consists of a multilayer array with m periods deposited on a substrate, as shown in Fig. 1. For instance, one period in

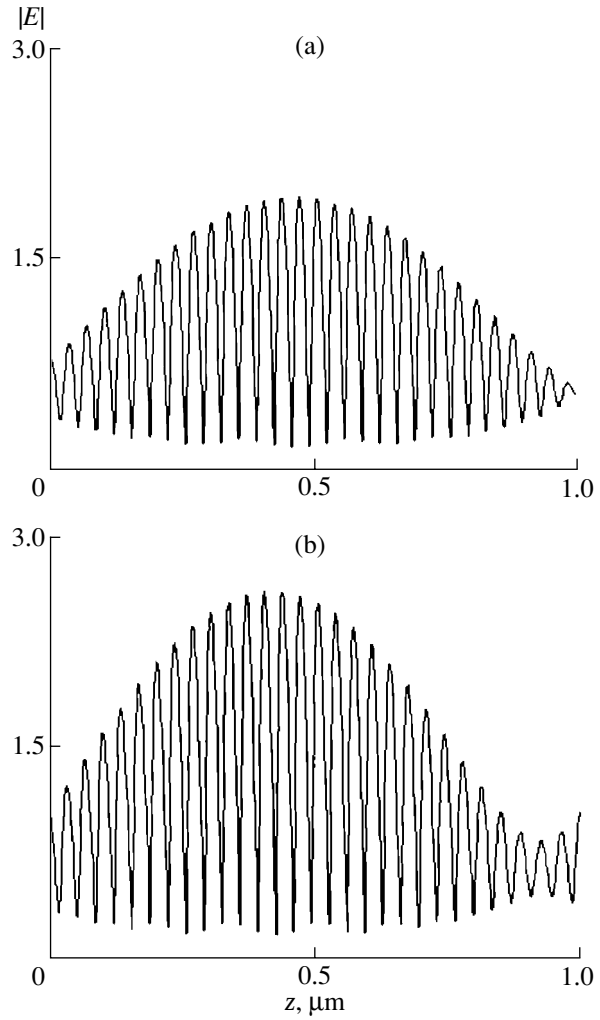

Fig. 3. The field amplitudes in the PGB. (a) GaAs substrate. (b) Air substrate. The wavelengths of the fields were chosen at the first transmission resonance on the long wavelength side of the band gap. The transmission maximum is different for the two cases: (a) 1074.4 nm and (b) 1075 nm.

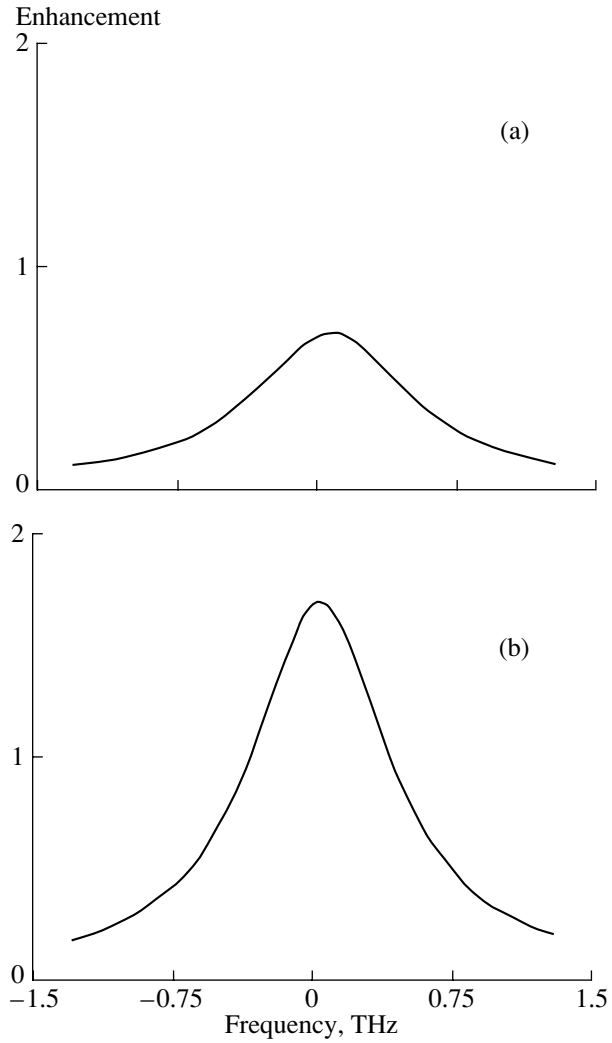

Fig. 4. Down-converted signal enhancement obtained for the samples from the field amplitudes in Fig. 3: (a) GaAs substrate and (b) Air substrate.

the structure consists of one layer of GaAs and one layer of AlAs, both a quarter-wave thick; i.e., the thickness of each layer was chosen to be a quarter wavelength of the light at the center of the band gap. A GaAs substrate is used, but we also explored eliminating the substrate and using an air interface on each side for comparison.

The calculated transmission spectra for a GaAs/AlAs quarter-wavelength stack are shown in Fig. 2. The design was chosen in such a way that the transmission peak on the long-wavelength edge of the band gap was close to one micron. In Fig. 2a, the GaAs substrate supports the PBG structure, and in Fig. 2b the substrate is removed. The layers thicknesses are d(GaAs) = 71.42 nm and d(AlAs)= 85.64 nm. The PGB stack has 30 periods (60 layers). A quick comparison of the transmission spectra shows that the large refraction index contrast for the air-substrate case generates higher transmission peaks. Correspondingly, calculation of the local fields in the structure when the field is tuned at the first transmission resonance reveals that the GaAs substrate has smaller resonant-field values in the PBG. The substrate affects the efficiency of the final microwave device design, as is demonstrated below.

The electromagnetic field amplitude inside the PBG structure is shown for two different substrate cases in Fig. 3. The wavelength is tuned to the first transmission resonance on the long-wavelength edge of the band gap. The peak values are reached at 1074.4 nm for the GaAs substrate and at 1075.7 nm for the air substrate. The GaAs substrate PGB structure has smaller field values, and, in both cases, the envelope of the field has a single maximum. For both cases, the field enhancement is modest but the maximum increases rapidly as more periods are added to the PBG. Also, we demonstrate below that large enhancements are possible with

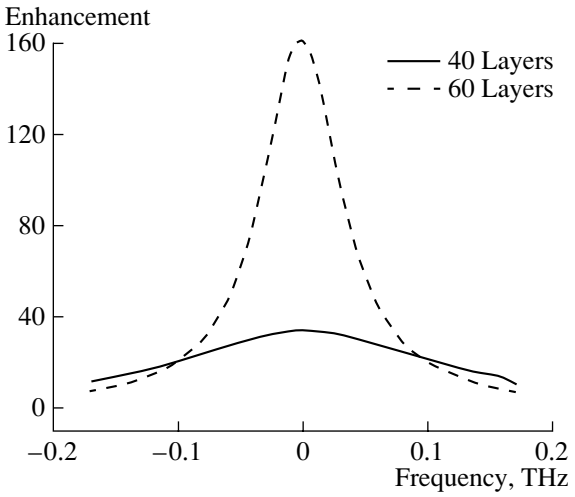

Fig. 5. Band-edge enhancement versus frequency plotted for two cases: 20 and 30 periods. In this case, a larger index contrast was used; each period is composed of GaAs/Al_2O_3 layers; the GaAs substrate is removed. The other parameters are discussed in the text. Note the difference of two orders of magnitude in the enhancement intensity (against Fig. 4b) obtained by the increasing index contrast.

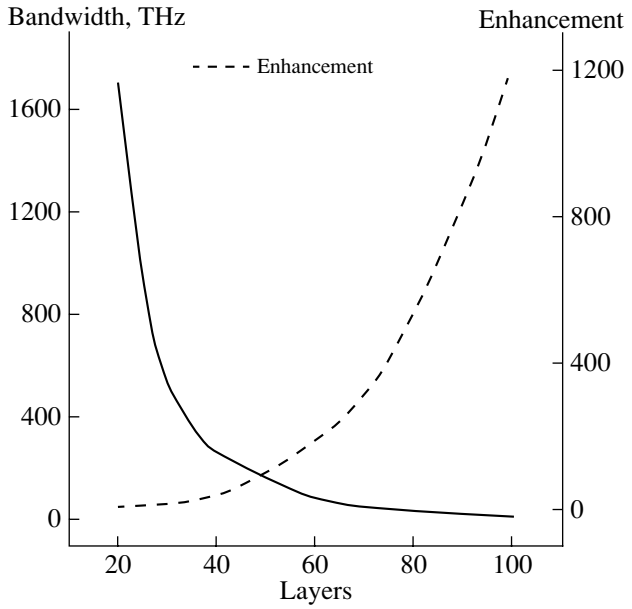

Fig. 6. Down-conversion signal enhancement and bandwidth versus the number of layer pairs for GaAs/Al_2O_3 PBGs. The parameters are the same as in Fig. 5.

added layers and when a defect is sandwiched between a pair of PBGs.

To generate THz radiation, two coherent fields are mixed in a second-order nonlinear material. The down-converted output signal is proportional to the product of the two fields inside the PBG sample. The thickness of the sample is much smaller than the wavelength of the down-converted signal, and propagation effects can be neglected. This also eliminates the need for phase matching of the fields. By taking the product of the fields at different wavelengths and integrating over the sample, we determine the sub-THz signal enhancement, which is expressed as

$$\eta = \frac{\left|\int_0^L E_1 E_2^* dz\right|^2}{L^2}. \quad (1)$$

The enhancement for GaAs and air substrates are extracted from Fig. 4. Both laser sources are normally incident on the PBG sample. The wavelength of one laser is fixed at the transmission maximum. The second laser is continuously tuned around the transmission maximum. The maximum occurs near the degeneracy frequency of the two lasers since the overlap of the field profiles is perfect. As the second laser is detuned, the overlap changes in both amplitude and phase and there is a sharp reduction in enhancement. The careful reader will observe that the field enhancement peak does not occur when both lasers are tuned to the same frequency (one laser remains tuned on the transmission maximum). This is because the maximum of the density of states is shifted slightly from the transmission maximum and this is manifest by a slight increase in the energy stored inside the PBG.

Eq. (1) is a crude measure that assumes a second-order nonlinearity to be the same in both materials. The normalization is the expected low-frequency signal when the sample is perfectly phase-matched in a homogeneous sample of the same length and same nonlinear coefficient. We have also extended this to the case when the second material does not possess a second-order nonlinear optical response to cover the alumina and air layer cases. In those samples, Eq. (1) is modified so that the integral only extends over the GaAs layers.

The enhancement is small for both cases in Fig. 4, with a depressed value for the enhancement when a GaAs substrate is used. It is about 58% smaller as compared to the air-substrate case. The bandwidth of the resonance is nearly 1 THz. As the number of periods is increased, the enhancement rapidly increases; however, on the other hand, the bandwidth of the resonance also decreases as more layers are added.

The band-edge enhancement for 20 and 30 periods is shown in Fig. 5, but in this case we have modified the index contrast of the layers changing the second material layer. The layer pairs are GaAs/Al_2O_3 with air for both the substrate and superstate. The thickness of each layer is d(GaAs) = 71.42 nm and $d(Al_2O_3)$ = 166.66 nm. For 40 layers (i.e., 20 periods), the THz signal enhancement is about 35; further increasing the number of layers by 50% results in an increase of the peak signal enhancement of about a factor of 4.

Also, we extract the reciprocal relation between the enhancement and bandwidth from the curves in Fig. 5;

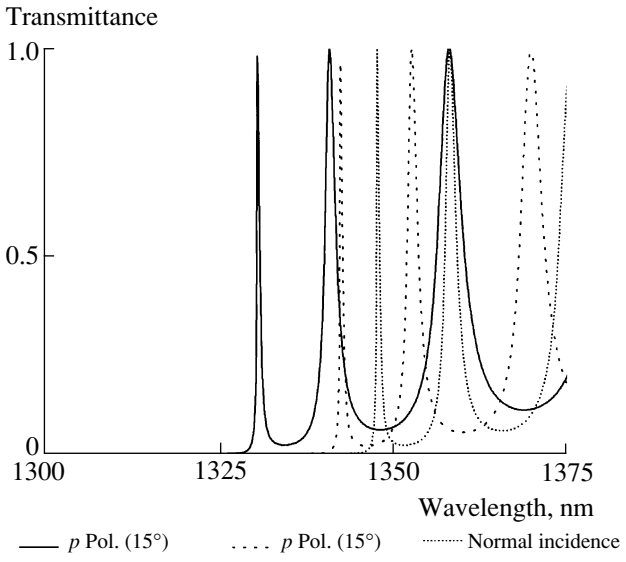

Fig. 7. Transmission spectra for normal incidence and an angle of incidence of 15 degrees. The *p*- and *s*-polarizations have different shifts of their band-edge resonance peaks, but the resonance width is nearly the same.

as the peak enhancement increases, the bandwidth decreases. The behavior of the frequency enhancement and the bandwidth versus the number of layers is plotted in Fig. 6. We used the same physical parameters as in Fig. 5. The enhancement is achieved at the cost of bandwidth. The bandwidth is around 250 GHz for about 40 layers and is reduced to a value around 71 GHz for 60 layers.

We now consider the field enhancement for the same number of periods (30) but for different index contrasts, i.e., GaAs/AlAs (Figs. 4a, 4b) and GaAs/Al_2O_3 (Fig. 5). Substituting Al_2O_3 (index 1.5 @ 1.4 μm) for AlAs (index 2.919 @ 1.378 μm), but keeping the GaAs substrate, produces more than an order of magnitude increase in the enhanced intensity for the same number of layers. The field enhancement for GaAs/Al_2O_3 is also much larger than the no-substrate case, for which the enhancement is shown in Fig. 4b. For GaAs/Al_2O_3, we also found a sharper resonance feature at the band edge of the transmission spectrum. In both cases, the signal enhancement only includes the GaAs material. Cases with air as the second material continue the trend toward realizing higher field enhancement with fewer layer pairs. To summarize, for the larger index contrast, we achieve larger field enhancement; however, at the same time, the resonance bandwidth is narrowed. Fewer layers means that the fabrication will also be simpler, since fewer layers need to be controlled.

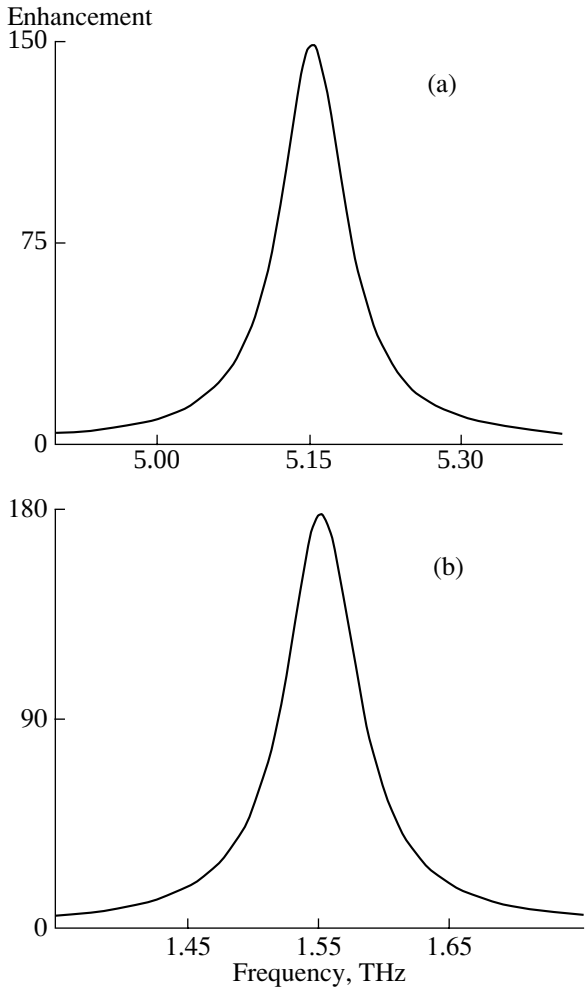

Fig. 8. Resonance enhancement of the THz signal for (a) *p*-polarization and (b) *s*-polarization. The peak is shifted into the THz regime, and the resonance width remains narrow.

2.2. Angle Tuning

The frequency of the down-converted signal can be tuned by intersecting two noncolinear laser sources. Suppose that one laser is normally incident on the medium and the second laser is nonnormally incidence, [2] which shifts the transmission maximum and the band edge. The same parameters are used here as for the dashed curve in Fig. 6 (N = 60, d(GaAs) = 71.42 nm, $d(Al_2O_3)$ = 166.66 nm). At nonnormal incident angles, the transmission spectrum is different for *p*- and *s*-polarizations. We find that the p-polarization has a much larger shift than the *s*-polarization for the same angle of incidence. Figure 7 displays the transmittance for normal incidence and the *p*- and *s*-polarizations incident at 15 degrees from the normal. The widths of both resonances do not appreciably change and the field enhancement inside the PBG structures is similar for both cases.

Figures 8a and 8b show that the overlap of the two fields is excellent and the enhancement is 150 and 180

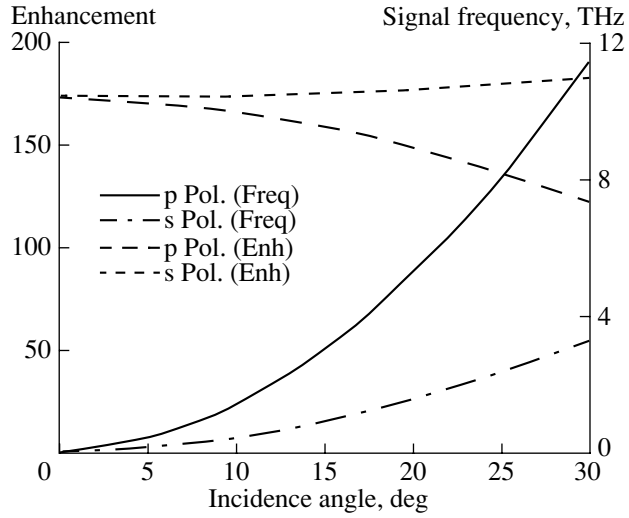

Fig. 9. Enhancement and signal frequency versus angle of incidence for *p*- and *s*-polarizations.

for *p*- and *s*-polarizations, respectively. The *p*-polarization has a maximum enhancement frequency at 5.15 THz, while for *s*-polarization the maximum is at 1.55 THz. Figure 9 highlights our results on the dependence of the THz emission with the angle tuning of the THz emission. The polarizations are degenerate at normal incidence and have their maximum near zero frequency. With tuning out to 30 degrees, the signal frequency at the maximum enhancement is about 11.5 THz for *p*-polarization and 3.5 THz for *s*-polarization. The peak enhancement for both polarizations remains over two orders of magnitude. The bandwidth of the enhancement peaks remains around 75 GHz over the entire range of angles.

2.3. Defect Enhancement

A localized defect mode can also be exploited as a mechanism to enhance THz signals in a PBG. Typically, a defect mode is established by placing a layer that is some multiple of a half-wave layer thickness between the quarter-wave multilayer stacks. Figure 10 illustrates the sample geometry for this case. The number of layers sandwiching the defect are not necessarily the same on each side. The sketch also includes the GaAs substrate.

As in the band-edge enhancement case, the defect enhancement is very sensitive to the number of layers (*M* for the top stack and *N* for the bottom stack in this case). For purposes of comparison, we have fixed *M* = 18 periods of GaAs/AlAs layers and N = 22 periods of AlAs/GaAs layers. Each period is made of two quarter-wave thickness layers. The thickness is 112.42 nm for the GaAs layers and 130.45 nm for the AlAs layers. The GaAs defect layer has a thickness of 1.349 nm, and the substrate is infinitely thick. These parameters were chosen for an available sample used for a different experiment. The gap lies in the infrared regime; it extends from 1400–1700 nm (the transmission spectrum for the sample is shown in Fig. 11). A defect mode is present in the center of the gap.

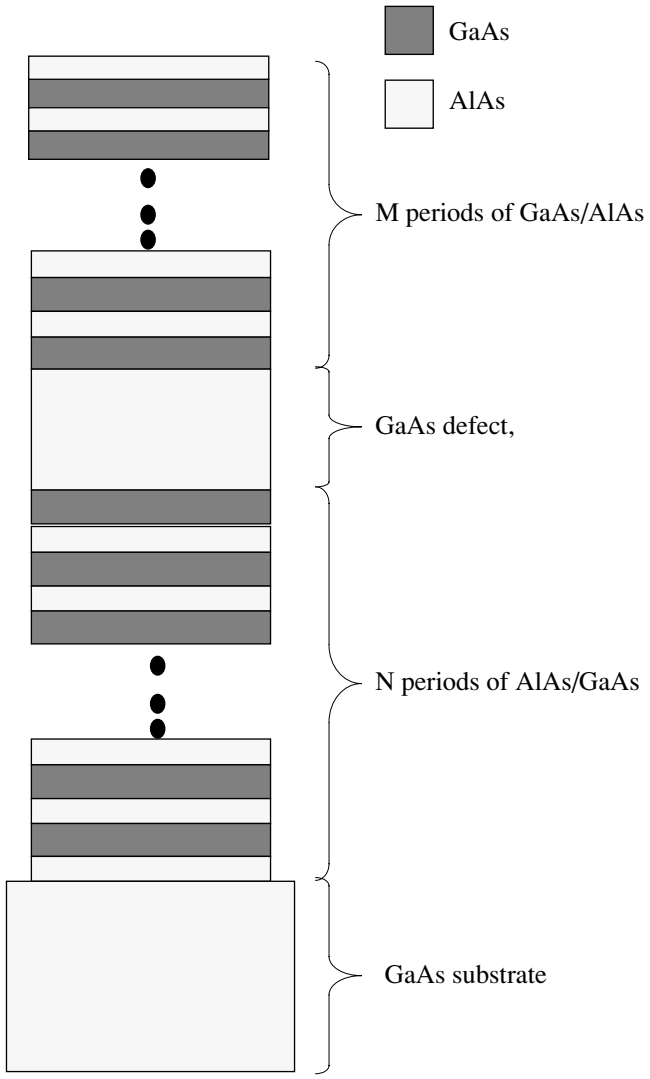

Fig. 10. Sample geometry with a defect layer sandwiched between two PBG stacks. The top PBG stack has M layers, and the bottom stack has N layers. The defect layer and the substrate are GaAs.

The transmission curve is very sharp at the defect-mode position, which peaks at 1518.87 nm. The plotting points were chosen on a grid with 0.05-nm spacing. Near the defect, the plotting points are separated by 0.01 nm. The defect mode in the center is sharp and has a large Q-factor. The local field distribution when one the wavelength of one of the driving lasers is tuned to the maximum transmission at the defect is shown in Fig. 12. The resonant intensity is increased by two orders of magnitude.

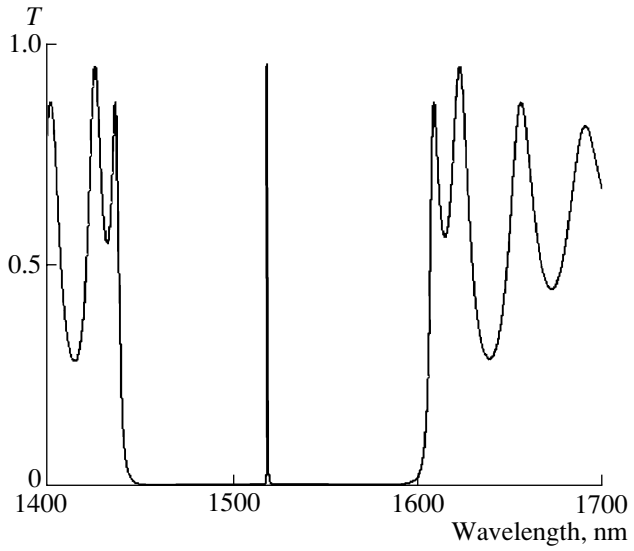

Fig. 11. Transmission spectra for a GaAs/AlAs sample with the defect mode shown in the band gap.

At normal incidence, the magnitude of the enhancement for this case is about 550. It represents an enhancement of almost three orders of magnitude over the band-edge enhancement case shown in Fig. 4. The resonant width of the enhancement peak is about 40 GHz, which is wide enough to minimize the laser bandwidth effects. However, by angle tuning one laser, we again observe a shift of the resonance position for both polarizations. The enhancement versus tuning frequency for an angle of incidence of 30 degrees is shown in Fig. 13. The shift is much smaller for our defect example than it was for the band-edge cases discussed in the previous section. At an angle of incidence of 30 degrees, the peak enhancement occurs at 2.3 THz but the size of the enhancement, about 420 for the p-polarization, remains large over the entire range of angles. The *s*-polarization shift is identical to the p-polarization shift in this case, and we do not separately plot that result. The bandwidth remains very narrow. By using larger angles of incidence, the frequency can be shifted to greater values but remains well below 10 THz out to angles of incidence of 80 degrees.

3. THz POWER CONVERSION

The power conversion efficiency can be roughly estimated for this process. The laser intensity and the THz intensity in free space are expressed in MKSA units as

$$I = \frac{c\varepsilon_0}{2}|E|^2. \tag{2}$$

Driving the THz signal with 1 mW of signal power focused on a spot area of 10^{-3} cm^2 yields an electric field amplitude of around 0.2×10^4 V/m. The THz field generated in the PBG is estimated from an approximate coupled-mode equation, whose expression is

$$E_{\mathrm{THz}} = \frac{2\pi}{\lambda}\chi^{(2)}\int_0^L E_1 E_2^* dz. \tag{3}$$

The THz intensity is given by

$$I_{\mathrm{THz}} = \frac{c\varepsilon_0}{2}\left(\frac{2\pi}{\lambda}L\right)^2 \eta(\chi^{(2)}E^2)^2. \tag{4}$$

For our estimate of the conversion efficiency, we use a sample length L = 10 μm, generated frequency λ =

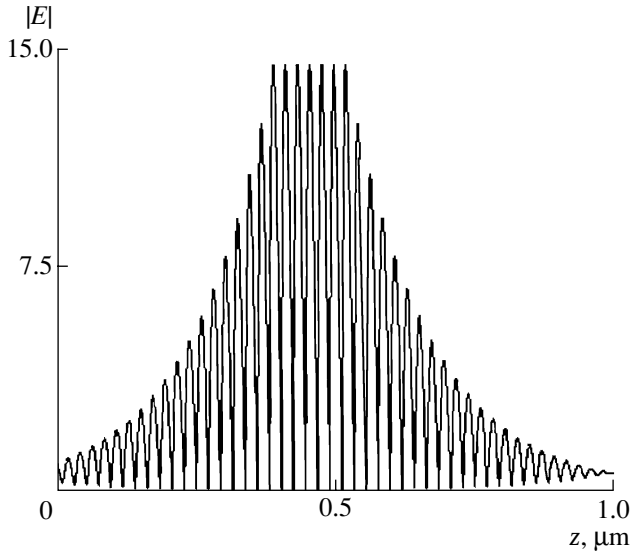

Fig. 12. Field amplitude in the PGB at the peak of the defect-mode transmission shown in Fig. 11.

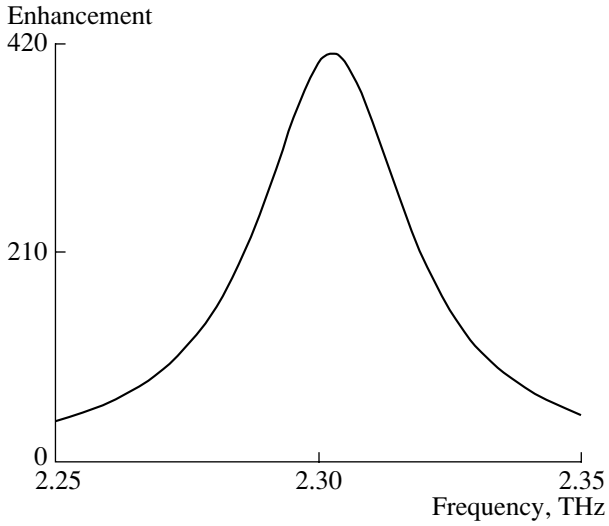

Fig. 13. Enhancement of the signal versus frequency. The angle of incidence of the second laser is 30 degrees. Only p-polarization is shown.

1 THz or $\lambda = 300\ \mu m$, $\chi^{(2)} = 10^{-11}$ m/V, and $\eta = 10^2$. The THz power generation is about 10 pW. The result scales in proportion to the pump power squared, so for 1-W laser powers the THz signal will be about 10 μW. The overall efficiency is inversely proportional to the THz wavelength, so higher frequencies will be generated with higher power. A large portion (more than two orders of magnitude) of the power inefficiency is due to the quantum efficiency of the down-conversion process.

4. CONCLUSIONS

We demonstrated that tunable, enhanced, long-wavelength signal generation from sub-THz to several THz is attainable using either band-edge or defect effects in a second-order nonlinear photonic band gap. By designing samples with specific numbers of layers and refractive index contrast, we can tune both the bandwidth and intensity of the signal. The excitation wavelengths are determined solely by the thickness of the layers and therefore can be tuned to wherever there are available sources.

For low refractive index materials, the signal enhancement increases by an order of magnitude for the same number of layers. We also find that a defect mode is very effective in providing large intensity enhancements, although the shift is not as large as the band-edge resonances. For our case of both *p*- and *s*-polarizations, the defect mode shifts by the same amount.

The enhancement values could enable us to obtain signals with GHz to THz frequencies and power levels
3 around 10 μW using 1-W cw lasers. The efficiency is enhanced over a small range of typically tens of GHz; however, a larger tuning into the THz range is achieved by angle tuning of the fields between two spectrally separated transmission resonances or defect modes.

ACKNOWLEDGMENTS

This work was supported by a DARPA grant, NSF grant ECS-0140109, and CONACyT no. 010470 through the program “Estancias sabáticas en el extranjero”. Also, one of the authors, MTC, would like to thank Prof. Haus and the EO program at UD for their hospitality.

SPELL: 1. detuned, 2. nonnormally, 3. cw

REFERENCES

1. T. W. Crowe, T. C. Grein, R. Zimmermann, and P. Zimmerrnann, IEEE Microwave Guid. Wave Lett. **6**, 207 (1996).
2. P. R. Smith, D. H. Auston, and M. C. Nuss, J. Quantum Electron. **24**, 255 (1988).
3. P. K. Benicewicz and A. J. Taylor, Opt. Lett. **18**, 1332 (1993).
4. M. A. Piestrup and R. N. Fleming, Appl. Phys. Lett. **26**, 418 (1975).
5. H. Minamide, K. Kawase, K. Imai, *et al.*, Rev. Laser Eng. **29**, 744 (2001).
6. A. Sato, K. Imai, K. Kawase, *et al.*, Opt. Commun. **207**, 353 (2002).
7. M. Bass, P. A. Franken, J. F. Ward, and G. Weinreich, Phys. Rev. Lett. **9**, 446 (1962).
8. K. H. Yang, P. L. Richards, and Y. R. Shen, Appl. Phys. Lett. **19**, 320 (1971).
9. L. Xu, X.-C. Zhang, and D. H. Auston, Appl. Phys. Lett. **61**, 1784 (1992).
10. S. L. Chuang, Phys. Rev. Lett. **68**, 102 (1992).
11. R. L. Aggarwal, B. Lax, H. R. Fetterman, *et al.*, J. Appl. Phys. **45**, 3972 (1974).
12. E. R. Brown, K. A. McIntosh, K. B. Nichols, and C. L. Dennis, Appl. Phys. Lett. **66**, 285 (1995).
13. A. M. Weiner and D. E. Leaird, Opt. Lett. **15**, 51 (1990).
14. A. Tredicucci, F. Capasso, C. Gmachi, *et al.*, Appl. Phys. Lett. **73**, 2101 (1998).
15. D. Grischkowsky, S. Keiding, M. van Exter, and Ch. Fattinger, J. Opt. Soc. Am. B **7**, 2006 (1990).
16. B. B. Hu and M. C. Nuss, Opt. Lett. **20**, 1716 (1995).
17. R. A. Cheville and D. Grischkowsky, Appl. Phys. Lett. **67**, 1960 (1995).
18. W. Sha, J. Rhee, T. Norris, and W. J. Schaff, IEEE J. Quantum Electron. **28**, 2445 (1992).
19. P. C. M. Brener, M. C. Planken, M. S. C. Nuss, *et al.*, J. Opt. Soc. Am. B **11**, 2457 (1994).
20. D. R. Dykaar and S. L. Chuang, J. Opt. Soc. Am. B **11**, 2454 (1994).
21. A. Godone and C. Novero, Metrologia **30**, 163 (1993).
22. Y.-S. Lee, T. Meade, M. DeCamp, *et al.*, Appl. Phys. Lett. **76**, 2505 (2000).
23. Yan-quing Lu, Min Xiao, and G. J. Salamo, J. Quantum Electron. **38**, 481 (2002).
24. M. Scalora, M. J. Bloemer, A. S. Manka, *et al.*, Phys. Rev. A **56**, 3166 (1997).